



Solvato(fluoro)chromism, investigation of quenching mechanism and thermodynamic binding parameter of two azine based chemosensor for Cu²⁺ ion, application in onsite detection

Bhriguram Das^{a,d}, Anamika Dhara^b, Subhabrata Mabhai^c and Satyajit Dey^{*a}

^aDepartment of Chemistry, Tamralipta Mahavidyalaya, Purba Medinipur-721 636, West Bengal, India

^bDepartment of Chemistry, Jadavpur University, Kolkata-700 032, India

^cDepartment of Chemistry, Mahisadal Raj College, Purba Medinipur-721 628, West Bengal, India

^dSubhaspalli Kunjabehari Vidyabhaban, Heria, Purba Medinipur-721 430, West Bengal, India

E-mail: satyajitdeyoc@gmail.com

Manuscript received online 29 July 2020, accepted 25 August 2020

Two solvatochromic fluorescent azine derivative 1-((*E*)-((*Z*)-(4-(diethylamino)-2-hydroxybenzylidene)hydrazono)methyl)naphthalen-2-yl (L1) and (*E*)-2-((4-(diethylamino)-2-hydroxybenzylidene)amino)-3',6'-dihydroxyspiro[isindoline-1,9'-xanthen]-3-one (L2) was synthesized via Schiff base condensation. The introduction of an electron-donating diethylamino group and an electron-accepting fluorophore unit into the pi-conjugated system of L1 and L2 endowed a prominent solvatochromic emission property. In contrast with the very little changes of absorption spectra in the different solvents, the emission was strongly dependent on the solvent polarity and could be tuned from blue region to red region by changing the solvent from less polar tetrahydrofuran to highly polar water. Both the ligand L1 and L2 were able to binds Cu²⁺ ion selectively via fluorescence turn-off process. The limit of detection (LOD) for Cu²⁺ was found to be 1.9 μM and 1.62 μM with L1 and L2, respectively. The photophysical experimental results reveal that the Cu²⁺ ions quenched the intrinsic fluorescence of both L1 and L2 by forming the ligand-metal complexes, but the quenching process different (static or dynamic) for the two probes. In addition, the binding spontaneity was mainly entropy-driven. Again both ligands successfully detect Cu²⁺ by means of TLC paper as well as simple filter paper based strips and hence, they would be very useful for onsite detection purpose.

Keywords: Solvato(fluoro)chromism, Cu²⁺ ion, quenching, LOD, thermodynamic spontaneity, paper strips.

Introduction

Luminescent materials derived from Schiff base compounds have attracted great attention in the past few decades owing to their potential applications in the fields of organic electronics, optoelectronics, sensors and informational displays¹. It is well known that the absorption and emission spectral responses of chemical compounds may be influenced by the surrounding medium and that medium can bring about a change in the position, intensity, and shape of absorption and/or emission bands. Hantzsch later termed this phenomenon solvatochromism^{2,3}. The term often solvatofluorochromism was defined for the emission position change upon solvent polarity variation. Obviously, this phenomenon is caused by differential solvation of the ground and first excited state of the light-absorbing molecule (or its chromophore). Differential solvation of these two states is

responsible for the solvent influence on emission spectra⁴. In general, molecules with a large change in their permanent dipole moment upon excitation exhibit a strong solvatochromic behaviour⁵. Besides the dipole moment change on excitation, the ability of a solute to donate or to accept hydrogen bonds to or from surrounding solvent molecules in its ground and Franck-Condon excited state determines further the extent and sign of its solvatochromism^{4,6,7}.

Fluorescent molecules possessing solvatochromic properties display different emission spectra depending on solvent polarity whose fluorescence intensity, color, and wavelength are sensitive to the environment^{5,8}. The absolute value of the red shift depends, usually linearly, on the solvent polarity. The more polar solvent with a higher static dipole moment polarizes molecules more strongly, the stronger the red shift. Due to their sensitivity to polarity and hydration,

solvatochromic dyes have been successfully applied to biological systems^{4,6}. Such fluorescent molecules can be used as polarity-sensitive molecular probes with non-destructive properties.

In addition, fluorescence quenching is one of the important phenomenon used in fluorescent chemical sensors, where the presence of small traces of a particular analyte is revealed by the decrease in emitted light intensity by a sensing probe^{9,10}. In any case, a variety of molecular interactions, viz. excited-state reactions, molecular rearrangement, energy transfer, ground state complex formation (static quenching) and collisional or dynamic quenching are responsible for sensing. Static and dynamic quenching can be differentiated by their different dependence on temperature and excited state life time. The classical Stern-Volmer model states that the lifetime is independent of quencher and remains unchanged ($\tau = \tau_0$) with the addition of quencher due to the formation of ground-state complexes. In addition, the quenching ratio should increase linearly with the quencher concentration as described by the Stern-Volmer equation. A similar linear behaviour is also predicted by the classical model in the case of pure collisional quenching, while a quadratic dependence with an upward curvature is expected in the presence of both mechanisms. However, positive deviation from linearity, i.e. upward curvature, was also frequently observed in systems involving only one of the two processes, either static or dynamic quenching. This has led to the introduction of a variety of second-order processes, such as in the "sphere of action" model or in the diffusion-limited treatment. Dynamic quenching is diffusion controlled because the quencher must diffuse to the fluorophore during the life time of excited state. Liu *et al.* and Mishra *et al.* recently separately reported two turn-off chemosensor for Cu²⁺ using unsymmetrical azine based Schiff base^{11,12}. However, the exact nature of quenching mechanism (static or dynamic) remains unclear. In this study, we have measured the fluorescence quenching in two Schiff base fluorophore **L1** and **L2**, interacting with the quencher Cu²⁺ ions, in a broad range of their respective concentrations and finalize the mechanism of quenching.

Again, thermodynamic parameters and the nature of binding forces responsible for the binding interaction¹³. The positive values of ΔH indicate that the processes are endothermic and binding between the metal ions and ligand is mainly

ΔS -driven, with little contribution from the enthalpy factor¹⁴. In this study, we have also investigated the nature of binding force operated in Cu²⁺ ion binding. Moreover, change in corresponding thermodynamic parameters did not investigate to explain the binding spontaneity. Herein, we have paid our attention on these issues by means of a number of spectroscopic studies. Again, the usefulness of the ligand for onsite Cu²⁺ detection has been checked by means of TLC paper as well as simple filter paper based strips.

Experimental

Material, method and measurements:

The chemicals were purchased from different commercial suppliers. Solvents used were of spectroscopic grade. 2-Hydroxy-1-naphthaldehyde ($\geq 99.0\%$), fluorescein ($\geq 97.0\%$), 4-*N,N*-diethylsalicylaldehyde (98.0%), Na₂EDTA (98.0%), hydrazine hydrate (98.0%) were purchased from Avra Scientific Ltd. The stock solutions of different metal ions were prepared in distilled water from their chloride (Na⁺, K⁺, Ba²⁺, Hg²⁺, Fe³⁺, Cr³⁺) or perchlorate (Mg²⁺, Mn²⁺, Cu²⁺, Co²⁺, Ni²⁺, Zn²⁺, Cd²⁺, and Pb²⁺) or nitrate salts (Ca²⁺, Al³⁺, Zn²⁺).

The electronic absorption and steady-state fluorescence spectra were obtained from a UV-Visible spectrometer (Model: Shimadzu UV, evolution 201) and a JASCO FP-8500 spectrophotometer equipped with a thermostated compartment, respectively. NMR spectra were taken on a Bruker DRX-400 spectrometer with tetramethylsilane (TMS) as an internal standard and CDCl₃ or DMSO-*d*₆ as a solvent. Mass spectra were recorded on Qtof Micro YA263 mass spectrometer. Melting point was measured on a local made apparatus in open capillary. Fluorescence lifetime was obtained by the method of Time Correlated Single-Photon Counting (TCSPC) using Horiba Yvon DeltaFlex Modular Fluorescence Lifetime System.

Synthesis of ligand L1 and L2:

Ligand **L1**: To an excess amount of hydrazine-hydrate (1 ml, 20 mol) the solution of 2-hydroxy-1-naphthaldehyde **1a** (345 mg, 2 mmol) in methanol was added and stirred overnight at room temperature. The excess solvent and hydrazine was removed by vacuum evaporation. The off white solid was washed with chilled methanol to get the product **1b**¹⁵. This product constituted the Schiff base having a mono-imine bond and a free amine group of hydrazine (Scheme 1). Calculated

lated yield was: 81%, m.p. 148–150°C, Elemental analysis: $C_{11}H_{10}N_2O$, Found (%): C, 70.88; H, 5.47; N, 15.08; O, 8.57. Calcd. (%): C, 70.95; H, 5.41; N, 15.04; O, 8.59; 1H NMR [400 MHz, $CDCl_3$, TMS, J (Hz), δ (ppm)] (Fig. S1): 12.28 (1H, s), 8.79 (1H, s), 7.99 (1H, d, J 8.4), 7.75 (2H, t, J 8.0), 7.5 (1H, t, J 8), 7.35–7.17 (2H, m), 5.53 (2H, s). In the next step, the mono-imine **1b** (186 mg, 1 mmol) was added to a solution of 4-*N,N*-diethylsalicylaldehyde (192 mg, 1 mmol) in methanol and stirred overnight. The solution volume was reduced to one third of initial to get an orange solid **L1**. The solid was washed with cold methanol several times to remove undesirable materials. Purity was checked by TLC paper (80:20 hexane:ethyl acetate, $R_f \sim 0.25$). Yield: 72%, m.p. 203–205°C Anal. Calcd. for Chemical formula: $C_{22}H_{23}N_3O_2$: C, 73.11; H, 6.41; N, 11.63; O, 8.85. Found: C, 73.87; H, 6.49; N, 11.16%; 1H NMR (Fig. S2, ESI) [400 MHz, $CDCl_3$] δ (ppm): 13.16 (1H, s), 11.69 (1H, s), 9.51 (1H, s), 8.57 (1H, s), 8.13–8.15 (1H, d, J 6.8 Hz), 7.77–7.83 (2H, dd, J 6.4 Hz, 7.2 Hz), 7.54–7.57 (1H, m), 7.36–7.39 (1H, t, J 6.0 Hz), 7.21–7.23 (1H, d, J 7.2 Hz), 7.14–7.15 (1H, d, J 7.2 Hz), 6.29–6.27 (1H, d, J 6.8 Hz), 6.247 (1H, s), 3.39–3.43 (4H, q, J 5.6 Hz), 1.2–1.23 (6H, t, J 5.6 Hz). MS (Fig. S3, ESI): m/z = 361.18 (calculated), 362.1864 (100.0%) $[M+H]^+$ (observed). IR (KBr, cm^{-1}) (Fig. S4, ESI): 3469 (-OH), 2970, 2368, 1629 (C=N), 1580, 1515, 1479, 1410, 1350, 1244, 1186, 1128, 1070, 946, 815.

Ligand **L2**: To an excess amount of hydrazine-hydrate (2 ml, 41.6 mmol) the solution of fluorescein **2a** (662 mg, 1.91 mmol) in methanol was added and refluxed for 8 h and then it was poured into ~200 ml of ice-cold water, kept for overnight. The off white precipitate formed was filtered, washed with water and chilled methanol thoroughly, and dried in vacuum to get the desired product **2b**¹⁶. Yield: 490 mg, m.p. 260°C. In the next step, to the methanolic solution of fluorescein hydrazine **2b** (250 mg, 0.72 mmol) the solution of 4-*N,N*-diethylsalicylaldehyde (140 mg, 0.72 mmol) in methanol was added. The mixture was refluxed for 8 h with simultaneous TLC monitoring. A very faint yellow solid appeared after reducing the volume of solvent to a quarter of its initial, and it was collected by filtration, washed repeatedly with chilled methanol to remove unwanted material. TLC shows its purity with 80:20 hexane:ethyl acetate (R_f 0.15). After drying the product ~78% yield was obtained (Scheme 1). m.p. 280–282°C, Elemental analysis: $C_{31}H_{27}N_3O_5$, Found (%): C, 70.88; H, 5.47; N, 15.08; O, 8.57. Calcd. (%): C, 71.39; H,

5.22; N, 8.06; O, 15.34; 1H NMR [600 MHz, $DMSO-d_6$, TMS, J (Hz), δ (ppm)] (Fig. S5): 10.43 (1H, s), 9.92 (2H, s), 9.0 (1H, s), 7.89 (1H, d, J 7.2), 7.61–7.58 (2H, t, J 7.2), 7.12 (1H, d, J 7.2), 7.02 (1H, d, J 9.0), 6.62 (2H, d, J 1.8). 6.48–6.45 (4H, dd, 8.4), 6.18–6.17 (1H, m), 3.33–3.327 (4H, q, J 6.6), 1.05–1.03 (6H, t, J 6.6); ^{13}C NMR [150 MHz, $DMSO d_6$, TMS, δ (ppm)] (Fig. S6, ESI): 162.7, 159.68, 158.58, 154.62, 152.22, 150.49, 150.04, 133.58, 132.06, 129.52, 129.09, 128.17, 123.61, 122.9, 112.42, 109.61, 106.27 103.81, 102.4, 97.33, 65.21 (spiro), 43.82, 12.43. m/z (Fig. S7) = 521.1951 (1H, d, J 1.2) (100.0%) (calculated), 521.2 (observed); IR (KBr, cm^{-1}); (Fig. S8): 3469 (-OH), 2970, 2368, 1629 (C=N), 1580, 1515, 1479, 1410, 1350, 1244, 1186, 1128, 1070, 946, 815.

Preparation of **L1-Cu²⁺** and **L2-Cu²⁺** complex:

The receptor **L1** (100 mg, 0.27 mmol) and Cu-perchlorate (112 mg, 0.31 mmol) salt were dissolved separately in methanol, and mixed together in a small round bottle. The mixed solutions were stirred overnight at room temperature and kept for solvent evaporation. After one week a grey solid obtained. This was characterized by ESI-MS and FTIR spectra. ESI-MS (Fig. S10): 441.8507 (obtained for **L1** - 2H + Cu^{2+} + H_2O + H^+), Calcd. m/z : 440.103 and 483.8832 (obtained for **L1** - 2H + Cu^{2+} + H_2O + CH_3CN + H^+), Calcd. m/z : 481.1301, 483.1283; IR (KBr, cm^{-1}) (Fig. S11, ESI): 3465, 2966, 1616, 1454, 1314, 1078, 793, 755.

The receptor **L2** (150 mg, 0.28 mmol) and Cu-perchlorate (102 mg, 0.28 mmol) salt were dissolved separately in methanol, and mixed together in a small round bottle. The mixed solutions were stirred overnight at room temperature and kept for solvent evaporation. After one week a grey solid obtained. This was characterized by ESI-MS and FTIR spectra. ESI-MS (Fig. S12): m/z 583.53, 601.54 and 631.72 correspond to [**L2** - H^+ + Cu^{2+}], [**L2** - H^+ + Cu^{2+} + H_2O] and [**L2** - H + Cu^{2+} + H_2O + CH_3OH]; IR (KBr, cm^{-1}) (Fig. S13, ESI): 3543 (-OH, broadened), 1622(C=N).

Photo-physical studies:

For UV-Vis absorbance and PL experiment, stock solution of **L1** and **L2** ($c = 1 \times 10^{-3}$ mol L^{-1}) was prepared in acetonitrile. Solutions of different metal cations ($c = 1 \times 10^{-3}$ mol L^{-1}) were prepared in water (20 μ M HEPES buffer, pH 7.2). For metal selectivity and titration experiment solutions of desired concentrations of probes and cations were prepared separately. For investigating metal ions selectivity of the sen-

for **L1** and **L2** and in titration experiments, quartz optical cell of 1 cm optical path length was filled with 2 mL solvent with 40 μ L of **L1** and **L2** (20 μ M) and the metal ions solutions were added to **L1** and **L2** using a micropipette. Each spectrum recorded at 298 K after 1 min of addition of the metal ion solution. For detailed steady state PL study excitation wavelength was set at 380 nm (Ex bandwidth 2.5 nm, Em bandwidth 5 nm) emission was acquired from 380 nm to 650 nm.

Fluorescence lifetime measurements:

Fluorescence lifetimes were measured by the method of Time-Correlated Single- Photon Counting (TCSPC) using a HORIBA Jobin Yvon Fluorocube-01-NL fluorescence lifetime spectrometer. The sample was excited using a laser diode at 375 nm and the signals were collected at the magic angle of 54.7° to eliminate any considerable contribution from fluorescence anisotropy decay^{17,18}. The typical time resolution of our experimental setup is ~100 ps. The decays were deconvoluted using DAS-6 decay analysis software. The acceptability of the fits was judged by χ^2 criteria and visual inspection of the residuals of the fitted function to the data. Mean (average) fluorescence lifetimes were calculated using the following equation¹⁹:

$$\tau_{av} = \frac{\sum \alpha_i \tau_i}{\sum \alpha_i}$$

in which α_i is the pre-exponential factor corresponding to the i -th decay time constant, τ_i .

Calculation of detection limit (LOD):

The detection limit was calculated from the fluorescence

titration using the equation¹²:

$$\text{Detection limit} = 3 \sigma/k$$

where σ is the standard deviation of blank measurement, and k is the slope between the fluorescence emission intensity versus $[\text{Cu}^{2+}]$. To obtain the slope, the fluorescence emission intensity at wavelength 543 nm (for **L1**) or 528 nm (for **L2**) was plotted as a function of the concentration of Cu^{2+} .

Preparation of paper based strips:

The test strips were made by absorbing the solution of **L1** and **L2** (10^{-3} M) on filter paper/thin layer chromatography paper using capillary glass at different separate place and air dried. Then, different metal ion solutions (10^{-2} M) were spotted on the previous spots, dried.

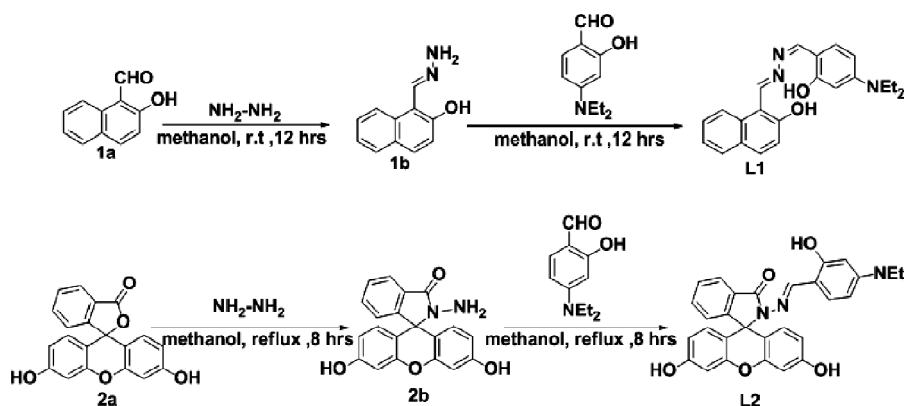
Results and discussion

Synthesis and characterization:

The target compound **L1** and **L2** was conveniently obtained from fluorescein, 2-hydroxy-1-naphthaldehyde and 4-*N,N*-diethylsalicylaldehyde via Schiff base condensation reaction in two steps (Scheme 1). All of the synthesized compounds were well characterized by ¹H NMR, ESI-MS, FTIR, and ¹³C NMR (see the Supporting Information).

Solvatochromism:

The probe **L1** and **L2** shows distinctive colored emission in various solvent under the light of UV-cabinet ($\lambda = 366$ nm) as shown in Fig. 1B, inset. With increasing solvent polarity, we observe different emission with the probe **L1** and **L2**. In non-polar or mild polar solvent-like tetrahydrofuran (THF), **L1** shows bluish PL and whereas with highly polar solvents



Scheme 1. Synthetic scheme for the probe **L1** and **L2**.

like acetonitrile (ACN), dimethylformamide (DMF), ethanol (EtOH), methanol (MeOH) and water (H₂O) the probe shows greenish PL although the absorption spectral position remains same for several solvent except in water where slight red shifting occurs (Fig. 1A-B). The shift in emission spectral position from 475 nm to 528 nm indicates the probe is solvatochromic. The probe **L2** shows distinct emission in various solvents under the light UV chamber ($\lambda = 366$ nm) as shown in Fig.1C, inset. Using different solvent with increasing solvent polarity, we get different emission shift with the probe **L2**. In non-polar or mild polar solvent like THF, **L2** shows bluish PL and with highly polar solvent like ethanol, methanol, water the probe shows reddish PL, although there is no marked change in absorption maxima with different polar solvents. The shift in PL intensity from 521 nm to 558 nm makes the probe solvato (fluoro)chromic (Fig. 1C-D).

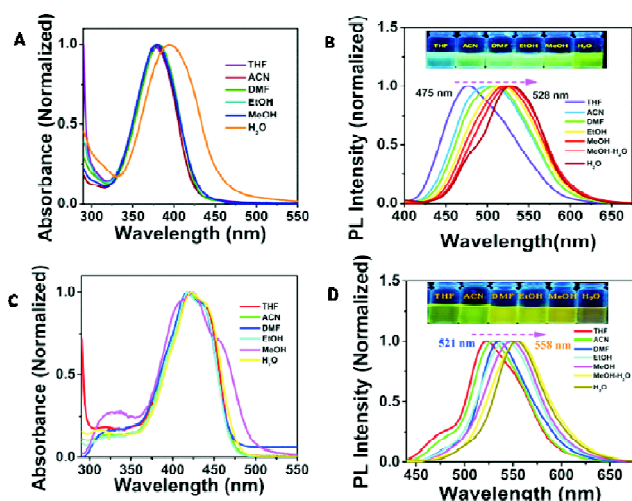


Fig. 1. (A,C) Solvent effect on absorbance of **L1**, **L2** (B,D) solvent effect on emission of **L1**, **L2** ($\lambda_{\text{ex}} = 380$ nm). inset: corresponding photographic image under UV-lamp ($\lambda = 366$ nm).

Selective Cu²⁺ sensing via fluorescence quenching:

Both the ligand **L1** and **L2** capable to binds Cu²⁺ ion strongly shown in absorption spectra (Fig. S9A-S9B) which was successfully described by two groups with these ligands^{11,12}. Again they also represent selective turn off Cu²⁺ sensing which was verified our group (Fig. 2A-2D). The ligand **L1** and **L2**, both show turn off sensing knack towards Cu²⁺ in all the solvent we used. We take acetonitrile for the study as its polarity index lies in between less polar solvent THF and

highly polar water [polarity index value for THF = 4, MeOH = 5.1, EtOH = 5.1, MeCN = 5.8, DMF = 6.4 and H₂O = 9.0]. Separate addition (10 equiv.) of Na⁺, K⁺, Ba²⁺, Mg²⁺, Ca²⁺, Mn²⁺, Cu²⁺, Al³⁺, Fe³⁺, Cr³⁺, Co²⁺, Ni²⁺, Zn²⁺, Cd²⁺, Hg²⁺ and Pb²⁺ solutions to the solution of **L1** (20 μ M) followed by fluorescence spectra recording shows that the fluorescence of **L1** was quenched selectively with only Cu²⁺ (Fig. 2A) over the other metal ions, which was observed even with naked eyes under UV-cabinet (Fig. S14A, inset). Similar observation was also noted from ligand **L2** (Fig. 2B).

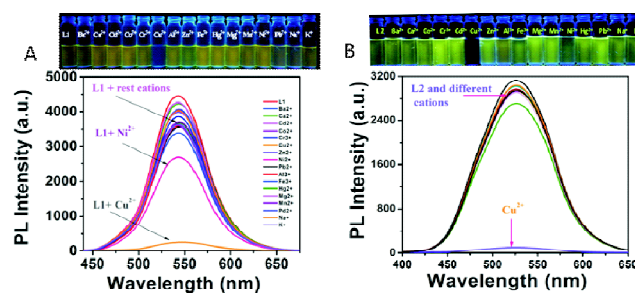


Fig. 2. Metal ion selectivity study by fluorescence spectra for (A) ligand **L1** and (B) ligand **L2** ($\lambda_{\text{ex}} = 380$ nm).

To gain deep insight in binding and sensing phenomenon absorbance as well as fluorescence titration were performed with Cu²⁺ for both **L1** and **L2**. With the gradual addition of Cu²⁺ to the solution of **L1**, systematic decrease in the absorbance at 416 nm with simultaneous increments near 470 nm (Fig. 3A) was observed. Again, in case of **L2**, addition of Cu²⁺, ~48 nm bathochromic shift from 384 nm to 432 nm along with formation of two clear isosbestic point at 330 nm and 403 nm (Fig. 3B) was noticed. This two titration results indicates both ligand **L1** and **L2** undergoes new complex formation with Cu²⁺ addition.

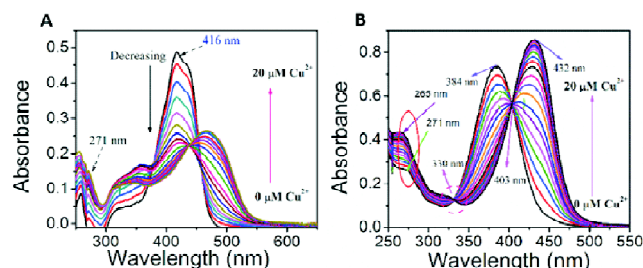


Fig. 3. Absorption titration plot of (A) **L1** (20 μ M) with Cu²⁺, (B) **L2** (20 μ M) with Cu²⁺.

Again, the incremental addition of Cu^{2+} to the solution of **L1** readily decreases the emission intensity without marked shifting of emission wavelength from 543 nm (Fig. 4A). The limit of detection for chemosensor **L1** as a fluorescent sensor for Cu^{2+} detection was determined from a plot of fluorescence intensity as a function of Cu^{2+} concentration. It was found that chemosensor **L1** has a limit of detection of 1.9 μM (Fig. 4B). Similarly, the titration for **L2** with incremental addition of Cu^{2+} reveals the regular decrease of emission intensity at 528 nm (Fig. 4C). The LOD value for Cu^{2+} with **L2** was calculated to be 1.62 μM (Fig. 4D). Both the detection limit was below from the recommended range (1.3 mg/L) by USEPA (Unites States Environmental Protection Agency).

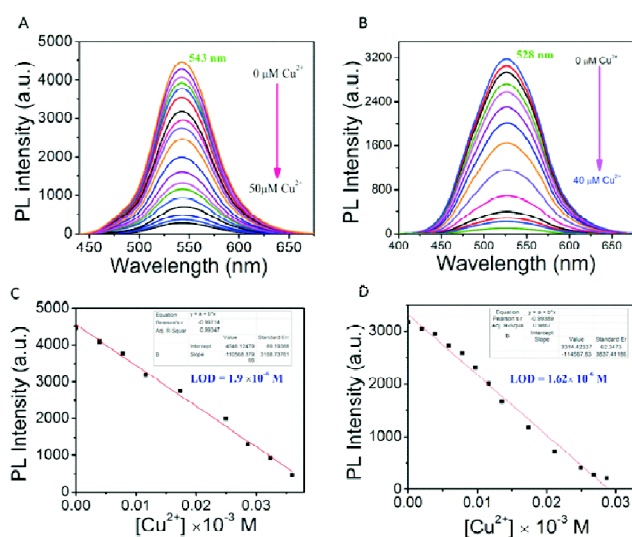


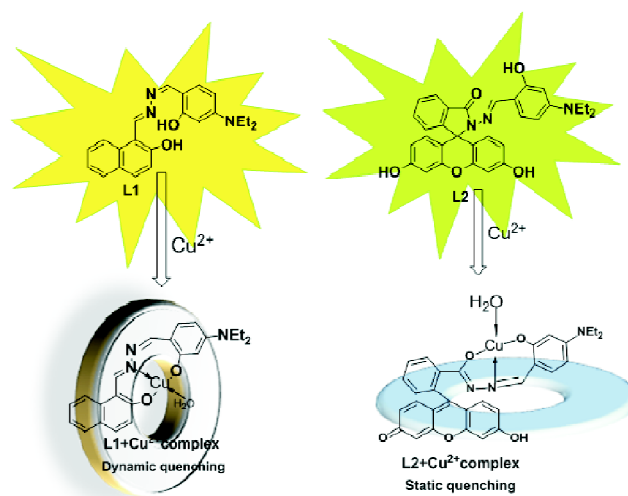
Fig. 4. Fluorescence titration plot of (A) **L1** (20 μM) with Cu^{2+} , (B) **L2** (20 μM) with Cu^{2+} ($\lambda_{\text{ex}} = 380 \text{ nm}$), (C) Linear regression plot for detection limit calculation for **L1** and (D) Linear regression plot for detection limit calculation for **L2**.

Binding and sensing (quenching) mechanism of **L1** and **L2**:

The recognition of Cu^{2+} with **L1**, and Cu^{2+} with **L2** was confirmed from Mass spectra (Figs. S10, S11) as well as from FTIR spectral analysis (Figs. S12, S13). The peak at 441.8507 obtained for $[\text{L1} - 2\text{H} + \text{Cu}^{2+} + \text{H}_2\text{O} + \text{H}^+]$ and 483.8832 obtained for $[\text{L1} - 2\text{H} + \text{Cu}^{2+} + \text{H}_2\text{O} + \text{CH}_3\text{CN} + \text{H}^+]$. Again, FTIR spectral shift to 3465 cm^{-1} (broad) from 3479 cm^{-1} and to 1616 cm^{-1} from 1629 cm^{-1} confirms strong binding. The mass analysis of **L2**- Cu^{2+} complex shows the peak

at 583.53, 601.54 and 631.72 correspond to $[\text{L2} - \text{H}^+ + \text{Cu}^{2+}]$, $[\text{L2} - \text{H}^+ + \text{Cu}^{2+} + \text{H}_2\text{O}]$ and $[\text{L2} - \text{H} + \text{Cu}^{2+} + \text{H}_2\text{O} + \text{CH}_3\text{OH}]$ complex formation.

The ^1H NMR spectra of the complex (we tested with both **L1**- Cu^{2+} and **L2**- Cu^{2+}) shows a broad proton signal at $\delta = 10.3 \text{ ppm}$ (-OH) with low integration value upon the addition of Cu^{2+} (Figs. S14, S15). The proton signal (imine) at $\delta = 8.02 \text{ ppm}$ (for **L1**- Cu^{2+}) and 8.9 ppm (for **L2**- Cu^{2+}) became broader as Cu^{2+} was added, indicating that Cu^{2+} binds to the nitrogen atom at the imine bond. Due to the paramagnetic nature of Cu^{2+} present in the complex fail to give detectable NMR signals or give very broad, poorly resolved signals as a consequence of rapid nuclear spin relaxation induced by the paramagnetism²⁰⁻²². The characteristic stretching frequency of C=O bond of the **L2** at 1633 cm^{-1} is shifted to a lower wavenumber at 1622 cm^{-1} in **L2**- Cu^{2+} complex indicating a binding through imine N-atom. IR stretching frequency of O-H bond of **L2** at 3435 cm^{-1} is shifted to 3543 cm^{-1} with broadening the signal upon addition of Cu^{2+} indicating the possibility that the oxygen of O-H group involves in co-ordinate bonding interaction as shown in the Scheme 2. The strong emission of both probes **L1** and **L2** are due to the presence of -OH and - NEt_2 donor groups in conjugation, which increases the electron density and also the lifetime of the excited fluorophore. The electron cloud of the excited fluorophore deformed as the Cu^{2+} ion formed a tightly bound complex at the receptor end. Due to the paramagnetic nature of Cu^{2+} the non-radiative decay becomes increasingly significant with Cu^{2+} bounded receptor, and



Scheme 2. Probable binding and quenching mechanism.

hence fluorescence quenching also becomes much more efficient^{23,24}. These experimental data reveals the probe **L1** and **L2** quenched by Cu^{2+} due to CHEQ effect. Out of two quenching path (static and dynamic quenching), in our probe, there was two distinct trends for **L1** and **L2**. To understand the possible mechanism of our detection system, we attempted to fit Stern-Volmer relationship to describe the concentration of Cu^{2+} ions and temperature dependence on the luminescence intensity of **L1**, **L2**. Fig. 5 shows the Stern-Volmer analysis of the quenching experiment (F_0/F versus $[\text{Cu}^{2+}]$). It is interesting to note the non-linear nature of the Stern-Volmer plot over the Cu^{2+} ions concentration ranges of 0–20 μM was observed with our probe. Several explanations of positive derivations from Stern-Volmer behavior have been advanced^{25,26}. One most commonly used is that a ‘static’ quenching mechanism is important at higher quencher concentrations. Again, the temperature effects on emission intensity are very helpful for predicting the exact mechanism of quenching^{27,28}. If such Stern-Volmer plots are obtained as a function of temperature, a determination might be made from the change in slope. As shown in Table 1, increased temperature often causes the slope (K) to increase for the probe **L1** indicating the dynamic quenching process is operated. In another case (for probe **L2**) the slope (K) decreases with increasing temperature indicating the quenching is static^{29–31}.

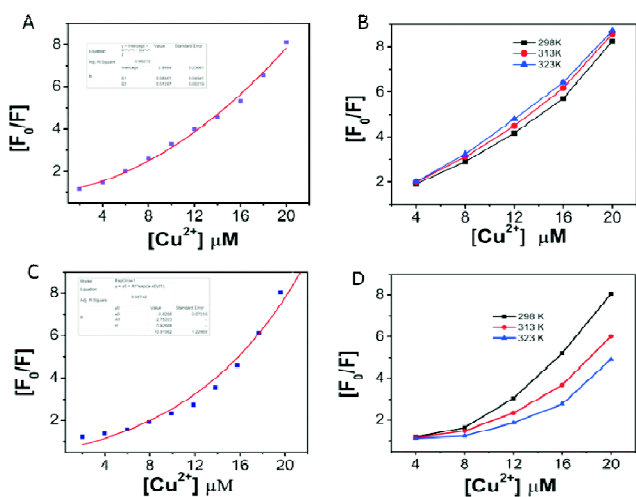


Fig. 5. (A) Stern-volmer plot at 298 K for **L1**, (B) temperature effect on Stern-Volmer plot for **L2**, (C) Stern-Volmer plot at 298 K for **L2** and (D) temperature effect on Stern-Volmer plot for **L2** ($\lambda_{\text{ex}} = 380 \text{ nm}$).

Temperature	298 K	313 K	323 K
K_{sv} for L1	38.7×10^4	40.5×10^4	41.4×10^4
K_{sv} for L2	43.2×10^4	29.8×10^4	22.7×10^4

To further study the quenching process, time-correlated single-photon counting (TCSPC) experiments have been used to test the charge transfer and exciton recombination process of **L1** and **L2**, in the presence and absence of Cu^{2+} ions. The fluorescence decay behavior in the absence and presence of Cu^{2+} is shown in Fig. 6A-6B and the exponential fit results are summarized in Fig. 6 (inset table) for the probe **L1** and **L2**. In the absence of Cu^{2+} , the fluorescence decays of **L1** being double exponentially by 0.07 and 1.42 ns time constants, which is the lifetime of the S1 state of free receptor **L1**. The lifetime of **L1** is found to be 1.29 ns. After 10 equiv. of Cu^{2+} is added into a buffer solution of **L1**, the fluorescence decays mostly by 0.09 and 1.88 ns time constants. The average luminescence lifetime of the **L1-Cu²⁺** system decreased to 0.40 ns, which is ascribed to the chelation quenched fluorescence (CHQF) process via dynamic quenching pathway.

Lifetime study in Fig. 6B shows that before and after introducing Cu^{2+} ions to **L2** solution, the average fluorescence lifetime remained almost the same (0.61 ns and 0.57 inset: Table). The suggestion is that, in this case, the mechanism of the quenching process involves complexation (static quenching) rather than collisional deactivation (dynamic quenching). Static quenching will not reduce the lifetime of the sample since those fluorophores which are not complexed – and hence are able to emit after excitation – will have nor-

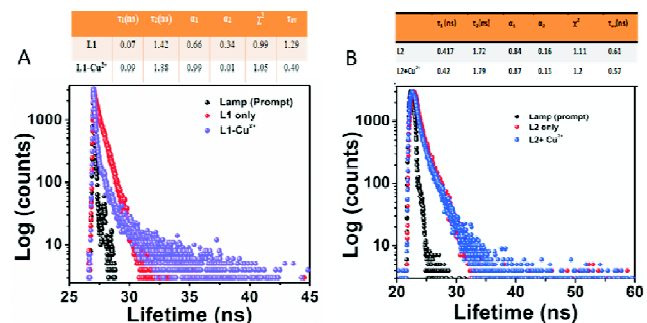


Fig. 6. Time-resolved fluorescence decay of (A) **L1** (red), **L1-Cu²⁺** (violet), (B) **L2** (red), **L2-Cu²⁺** (blue) and prompt (black) ($\lambda_{\text{ex}} = 372 \text{ nm}$).

mal excited state properties. The fluorescence of the sample is reduced since the quencher is essentially reducing the number of fluorophores which can emit. The static quenching mechanism for the probe **L2** is in the form of molecular association as $F_0/F > \tau_0/\tau$.

Binding constant and thermodynamic parameters:

In order to further elucidate the interactions between **L1** and Cu^{2+} ions, the binding constant was investigated at two different temperatures (298 K and 313 K) and the thermodynamic parameters, the enthalpy changes (ΔH), the entropy changes (ΔS) and the free energy changes (ΔG), were also calculated using the following well-known thermodynamic equations.

$$\ln(K_2/K_1) = (1/T_1 - 1/T_2)\Delta H/R$$

$$\Delta G = -RT \ln K$$

$$\Delta G = \Delta H - T\Delta S$$

where K is the binding constant at the corresponding temperature, R is the gas constant and T_1 , T_2 and T is the experimental temperature. From the thermodynamic parameters for the interaction between **L1** and Cu^{2+} ions in Table 2, the positive ΔH values showed that their interaction was an endothermic process (as with increase of temperature, binding constant decreases), the negative values ΔG indicated their binding process was spontaneous^{13,32}. The positive ΔS values exhibited the chelating properties between **L1** and metal ions and their binding was mainly ΔS -driven. This causes an increase in the entropy of the solvent, since the water and solvent surrounding an ion is oriented to a degree which depends on the ionic charge and the distance from the charged center, and most, (if not all) of this order is lost in chelate formation¹³. It is apparent that there is an increase in the number of molecules in chelate formation, and hence increases the entropy in the formation of the copper chelate. Similar conclusion regarding thermodynamics may also be drawn for the probe **L2**.

Table 2. Thermodynamic parameters (ΔH , ΔG and ΔS) of **L1**- Cu^{2+} system

Temp. (K)	ΔH (kJ mol ⁻¹)	ΔG (kJ mol ⁻¹)	K_a (mol ⁻¹)	ΔS (J mol ⁻¹ k ⁻¹)
298	47.643	-20.301	0.481×10^4	0.2354
313		-26.199	2.357×10^4	0.2359

Practical application of the sensor: Onsite detection:

The probe **L1** as well as **L2** shows bright yellowish emission when kept holds in UV-lamp in different solvent as well as in solid state, and also in filter/TLC paper. Different metal ion solutions (10^{-2} M) were spotted on the previously made spots with **L1** and **L2** separately, dried. The filter paper shows yellow color at most of the spots in ambient light, however a minute difference at Cu^{2+} (Fig. 7A, 7C). Remarkably, the spot at Cu^{2+} became darken when expose the paper to UV-light (366 nm), whereas all other spots illuminating yellow color yet (Fig. 7B, 7D). Therefore, the probe **L1** could be useful for onsite Cu^{2+} detection exclusively without requirement of any sophisticated high costly instruments. From these two experiments, it was clearly seen that the probe **L1** and **L2** displayed yellowish green fluorescence and get quenched completely with Cu^{2+} under UV-light and thus could be useful for direct qualitative estimation of Cu^{2+} in practical laboratory.

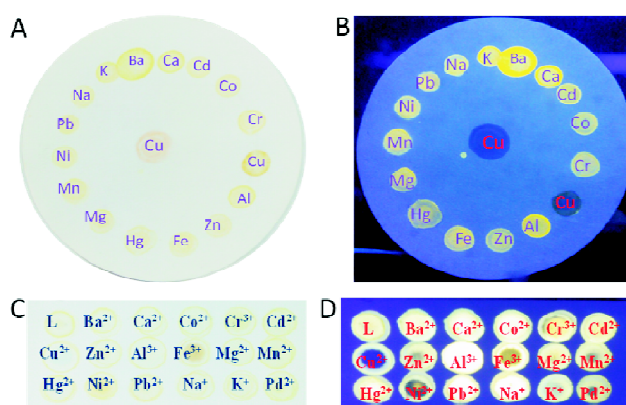


Fig. 7. Bare eye visualization of paper strips made using **L1** (top), **L2** (bottom) and different metal ions (A,C) under ambient light, (B,D) under UV-lamp ($\lambda = 366$ nm)

Conclusion

In this study, naphthol and fluorescein-based reliable two fluorescent chemosensor **L1** and **L2** have been synthesized for Cu^{2+} sensing mechanistic investigation. Both the ligand shows excellent intense color change from bluish/greenish to reddish with a 53 nm/45 nm bathochromic shift of the emission maxima in the emission spectrum by solvent polarity changing. The selective sensing ability of the probes towards Cu^{2+} ions through a turn-off fluorescence signaling mechanism occurred via dynamic and static quenching phenomena for **L1** and **L2**, respectively. The limit of detection

for Cu²⁺ was found to be 1.9 μM and 1.62 μM with **L1** and **L2**, respectively. The thermodynamic parameter reveals the binding of metal ion is associated with entropy favorable path. The complete quenching of the emission intensity was observed with Cu²⁺ ions in paper strips unravel the efficiency of the probe **L1** and **L2** to detect Cu²⁺ ions as an onsite sensor.

Acknowledgements

Authors thankful to the University Grants Commission, New Delhi, India, for financial support by sanctioning a minor research project (Sanction letter No. PSW-155/14-15 (ERO) ID No. WV6-027, S. No. 223832 dated 03-02-2015). We thank Dr. Asim Kr. Bera, Principal, Mahisadal Raj College and Dr. Abdul Motin, Principal, Tamralipta Mahavidyalaya for providing laboratory facilities.

References

1. T. L. Mako, J. M. Racicot and M. Levine, *Chem. Rev.*, 2018, **119**, 322.
2. A. Hantzsch, *Ber. Dtsch. Chem. Ges.*, 1922, 953.
3. E. S. Dodsworth, M. Hasegawa, M. Bridge and W. Linert, *Compr. Coord. Chem. II*, 2004, **2**, 351.
4. A. S. Klymchenko, *Acc. Chem. Res.*, 2017, **50**, 366.
5. A. Marini, A. Muñoz-Losa, A. Biancardi and B. Mennucci, *J. Phys. Chem. B*, 2010, **114**, 17128.
6. S. Nigam and S. Rutan, *Appl. Spectrosc.*, 2001, **55**, 362A.
7. A. A. Edwards and B. D. Alexander, "UV-Visible absorption spectroscopy, organic applications", Elsevier Ltd., 3rd ed., 2016.
8. C. Reichardt, *Chem. Rev.*, 1994, **94**, 2319.
9. J. M. V. Ngororabanga, C. Moyo, E. Hosten, N. Mama and Z. R. Tshentu, *Anal. Methods*, 2019, **11**, 3857.
10. A. T. Afaneh and G. Schreckenbach, *J. Phys. Chem. A*, 2015, **119**, 8106.
11. Y. Yang, F. Huo, C. Yin, Y. Chu, J. Chao, Y. Zhang, J. Zhang, S. Li, H. Lv, A. Zheng and D. Liu, *Sensors Actuators B: Chem.*, 2013, **177**, 1189.
12. R. Yadav, A. Rai, A. K. Sonkar, V. Rai, S. C. Gupta and L. Mishra, *New J. Chem.*, 2019, **43**, 7109.
13. M. Calvin and K. W. Wilson, *J. Am. Chem. Soc.*, 1945, **67**, 2003.
14. K. S. Siddiqi, S. Bano, A. Mohd and A. A. P. Khan, *Chinese J. Chem.*, 2009, **27**, 1755.
15. S. Samanta, S. Goswami, M. N. Hoque, A. Ramesh and G. Das, *Chem. Commun.*, 2014, **50**, 11833.
16. B. Das, A. Jana, A. Das Mahapatra, D. Chattopadhyay, A. Dhara, S. Mabhai and S. Dey, *Spectrochim. Acta - Part A: Mol. Biomol. Spectrosc.*, 2019, **212**, 222.
17. S. Banthia and A. Samanta, *J. Phys. Chem. B*, 2006, **110**, 6437.
18. B. Ramachandram and A. Samanta, *J. Phys. Chem. A*, 1998, **102**, 10579.
19. J. R. Lakowicz, "Principles of Fluorescence Spectroscopy", Plenum, New York, 1999.
20. J. T. Yeh, W. C. Chen, S. R. Liu and S. P. Wu, *New J. Chem.*, 2014, **38**, 4434.
21. P. S. Subramanian, E. Suresh and D. Srinivas, *Inorg. Chem.*, 2000, **39**, 2053.
22. N. Kato, M. Nakamura and T. Uchiyama, *J. Inorg. Biochem.*, 1999, **75**, 117.
23. K. Campbell, A. Zappas, U. Bunz, Y. S. Thio and D. G. Bucknall, *J. Photochem. Photobiol. A: Chem.*, 2012, **249**, 41.
24. H. Cho, J. B. Chae and C. Kim, *ChemistrySelect*, 2019, **4**, 2795.
25. E. Ciotta, P. Proposito and R. Pizzoferrato, *J. Lumin.*, 2019, **206**, 518.
26. F. Wang, Z. Gu, W. Lei, W. Wang, X. Xia and Q. Hao, *Sensors Actuators, B: Chem.*, 2014, **190**, 516.
27. W. E. Acree, *Zeitschrift fur Naturforsch. - Sect. A: J. Phys. Sci.*, 1993, **48**, 1265.
28. R. Giri, *Spectrochim. Acta - Part A: Mol. Spectrosc.*, 1992, **48**, 843.
29. S. Bano, A. Mohd, A. A. P. Khan and K. S. Siddiqi, *J. Chem. Eng. Data*, 2010, **55**, 5759.
30. M. Kasha, *J. Chem. Phys.*, 1952, **20**, 71.
31. M. Wang, K. Li, J. Hou, M. Wu, Z. Huang and X. Yu, *J. Org. Chem.*, 2012, **77**, 8350.
32. H. Liu, F. X. Li, Y. Pi, D. J. Wang, Y. J. Hu and J. Zheng, *Spectrochim. Acta - Part A: Mol. Biomol. Spectrosc.*, 2015, **145**, 588.